Applied Surface Science 409 (2017) 200–207

Contents lists available at ScienceDirect

Applied Surface Science

journal homepage: www.elsevier.com/locate/apsusc

Full Length Article

Electronic structure and STM imaging of the KBr-InSb interface

Piotr Ciochoń*, Natalia Olszowska, Jacek J. Kołodziej

Institute of Physics, Faculty of Physics, Astronomy and Applied Computer Science, Jagiellonian University, ul. prof. Stanisława Łojasiewicza 11, 30-348, Cracow, Poland

ARTICLE INFO

Article history:
Received 9 February 2017
Received in revised form 28 February 2017
Accepted 6 March 2017
Available online 7 March 2017

Keywords:
Thin film
Indium antimonide
KBr
Scanning tunneling
Microscopy
Interface

ABSTRACT

We study the properties of the InSb (001) surface covered with ultrathin KBr films, with a thickness of 1–4 ML. KBr deposition does not strongly perturb the crystallographic structure of the InSb surface and the electronic structure of the substrate also remains unaffected by the overlayer. A simple model of the studied system is proposed, in which a thin KBr layer is treated as a dielectric film, modifying potential barrier for the electrons tunneling to/from the InSb substrate. Apparent step heights on the KBr film, measured using scanning tunneling microscope (STM), agree well with the predictions of the model and the atomically-resolved STM images show the structure of the InSb-KBr interface. Our results demonstrate that STM may be used as a tool for investigations of the semiconductor–insulator interfaces.

1. Introduction

One of the most promising $A_{III}B_V$ semiconductors for applications in high-frequency electronics, spintronics and high-speed, low power digital logic applications [1,2] is indium antimonide (InSb). It is characterized by exceptionally high electron mobility ($7.7{\cdot}10^4\,cm^2V^{-1}s^{-1}$ at 300 K for pure intrinsic InSb) [3], small electron effective mass ($0.015m_e$ at the conduction band edge) and narrow band gap (0.17 eV at 300 K).

At the 2015 International Solid-State Circuits Conference (ISSCC) Intel has announced the plans to abandon silicon as the material used for its 7 nm process of fabricating field-effect transistors [4]; while no specific information was revealed, it is suspected that this means switching to fabrication of transistors based on $A_{III}B_V$ semiconductors [5]. Because of their exceptional electron transport properties, these materials allow for increased performance and reduced power consumption and are predicted to be the basis for the of the electronics of the future [6].

One of the requirements for the successful transition to electronics based on $A_{III}B_V$ compounds is the development of the reliable technology for the production of semiconductor/insulator systems. The native oxide layer grown on the compounds is usually characterized by low quality, making it unsuitable for applications [7,8], which results in the need of the introduction of other material on the surface. Alkali halides are model ionic insulators, which can be grown epitaxially on the (001) face of $A_{III}B_V$ semiconductor crystals, due to the strong bond between halogen atom and A_{III} atom on the surface of the substrate and due to the commensurate lattices of the compounds [9]. While these materials may not be the best candidates for insulating the gate in the future devices, since high-k materials technology may be relatively easily transferred to the fabrication processes based on the III–V semiconductors, they offer an exceptional opportunity to study crystallographically ordered semiconductor-ultrathin-dielectric (nano)systems. Even if the studied systems would not be applied in the devices directly, such studies may significantly advance the knowledge necessary for the development of the future electronic devices.

Quality of the interface between a semiconductor and an insulator can strongly affect the performance and electrical properties of the devices, through various mechanisms, (for example Fermi level pinning [10]). That makes it crucial to investigate and understand the structure of the interface, in order to gain a better control of the devices functionality. While some progress has been achieved in recent years in imaging the interface of epitaxial graphene with silicon carbide [11] and interface between alkanethiolate self-assembled monolayers on Au (111) surface using scanning tunneling microscopy [12], there is no established, direct method for the studies and imaging of interface structures.

For our studies we have chosen the closely-matched system of KBr – InSb(001) (InSb has the lattice constant 6.479 Å and KBr has the lattice constant 6.586 Å). We have studied the growth of

* Corresponding author.
E-mail addresses: ciochon.piotr@gmail.com, piotr.ciochon@doctoral.uj.edu.pl (P. Ciochoń).

http://dx.doi.org/10.1016/j.apsusc.2017.03.050
0169-4332/

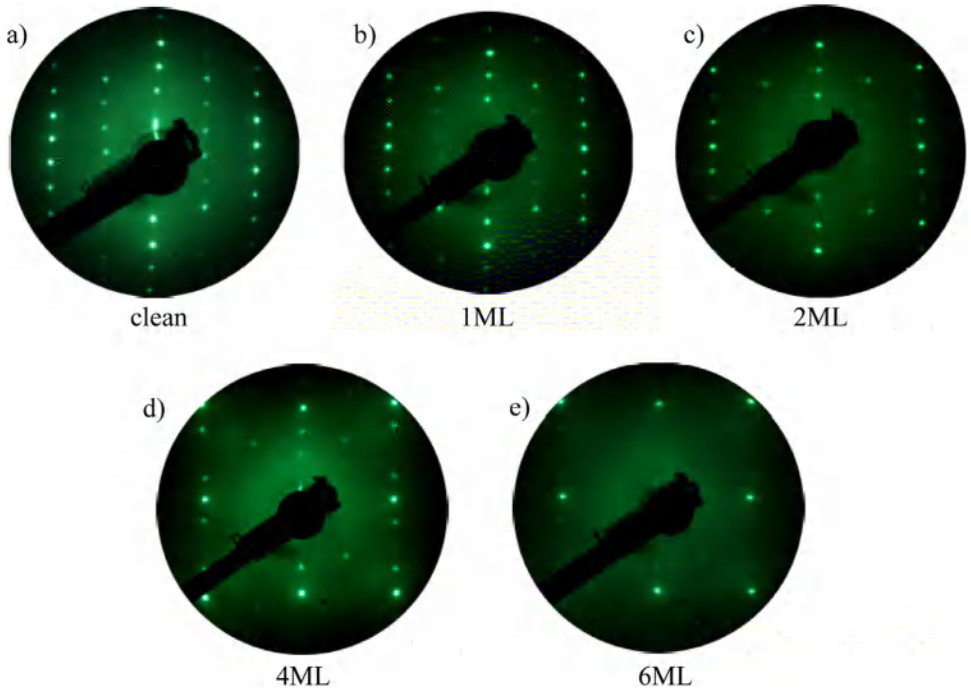

Fig. 1. Diffraction patterns of InSb (001) surface (incident electron energy E = 50 eV) with increasing KBr coverage (as indicated).

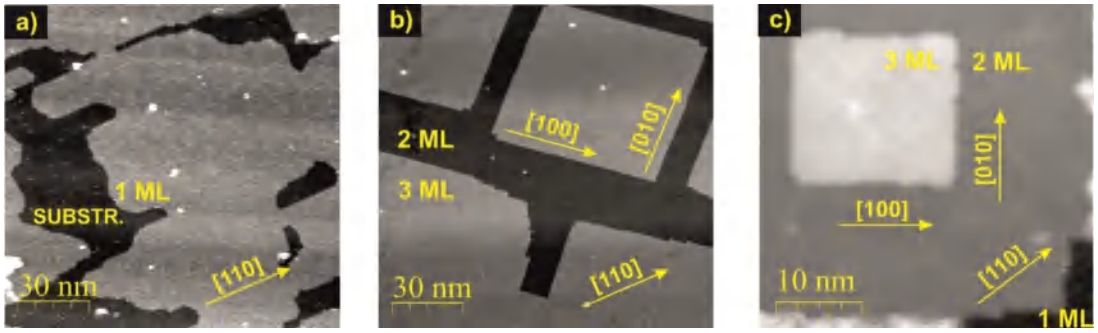

Fig. 2. STM images corresponding to different stages of KBr growth on InSb: a) growth of wetting layer, 0.75ML KBr coverage, tunneling current I = 10pA, sample bias U = −3.0 V, b)growth of the third layer, 2.5ML KBr coverage, tunneling current I = 50pA, sample bias U = −3.0 V, c)growth of third layer, 2.5ML KBr coverage, tunneling current I = 25pA, sample bias U = – + 4 V.

KBr films, their structure, as well as electronic properties of the KBr on InSb system, using low energy electron diffraction (LEED), angle-resolved photoelectron spectroscopy (ARPES) and scanning tunneling microscopy (STM). We will show that the formation of KBr band structure characteristic of the bulk material occurs already for ultrathin films, investigate KBr-InSb band alignment and show that, under certain conditions, the interface structure between KBr-InSb can be imaged directly using STM.

While the results are specific for the studied semiconductor-insulator interface, the approach may be possibly applied to other similar systems.

2. Materials and methods

Epi-ready, nominally undoped InSb wafers obtained from Mateck GmbH were initially annealed in UHV (base pressure $<1 \times 10^{-10}$mbar), at 427 °C, for several hours and then sputter cleaned at the same temperature, using rastered 700 eV Ar^+ ion beam (current density of 0.5–1 μA/cm^2, incidence angle 60° off normal). Sputtering cycles (duration of 1 h) were repeated until a clear c(8 × 2) LEED pattern was observed and, subsequently, final thermal annealing to 427 °C for 5 h was applied.

KBr was evaporated from a Knudsen effusion cell (operated at the temperature T = 450 °C) and deposited onto the substrates kept at the elevated temperature T = 100 °C, resulting in the constant KBr growth rate of 2.0 ML/min. (ML – single crystal layer parallel to (001) KBr, i.e. 4.6×10^{14} ion pairs per cm^2). The deposition rate was calibrated using quartz crystal microbalance (QCM) prior to each growth cycle and the actual surface coverage was calculated using growth time. In low coverages range microscopic observations allowed for independent estimation of KBr coverage, which was consistent with the QCM-derived values. The rest gasses pressure during deposition was kept below $<1 \times 10^{-9}$ mbar.

Clean, crystalline surfaces were imaged in constant current mode, using an Omicron LT STM microscope (electrochemically etched tungsten tips were used as probes), at temperatures ranging from 298 K down to 80 K. VG-SCIENTA R4000 hemispherical electron energy analyzer with a Heα – VUV5k UV lamp with monochromator tuned for a Heα line were used for angle-resolved photoelectron spectroscopy measurements, at T = 80 K. OCI MCP LPS300-D diffractometer was used for LEED studies.

3. Results and discussion

3.1. Surface structure – LEED, STM

Fig. 1 shows the evolution of the diffraction pattern of the InSb (001) surface with increasing coverage of KBr

The clean surface is characterized by the c(8 × 2), In-rich surface reconstruction (Fig. 1a), typical for the IBA preparation procedure. It has a very good crystallographic ordering and low defect concentration, as evidenced by sharp diffraction spots and high signal-to-noise ratio. The diffraction spots characteristic for the c(8 × 2) reconstruction lose relative intensity compared to (1 × 1) spots (Fig. 1b and d), but remain visible for increasing KBr coverages (up to 4ML). This suggests that the changes in the structure of the InSb surface covered with KBr are marginal – the change in the intensity is attributed mostly to the attenuation of electrons in the KBr layer. It is observed that the diffraction maxima in the half-order row appear to diminish in intensity slightly faster, but this effect does not appear to be significant and its explanation, requiring the analysis of the complex processes of electron multiple-scattering in thin films, is beyond the scope of this paper. For coverages ≥6ML, (1 × 1) reconstruction, associated to KBr surface becomes dominant and any signal associated to the sub-surface c(8 × 2) reconstruction is lost (Fig. 1e).

STM observations of the growth of KBr films on InSb(001) are particularly clear to interpret which is due to the fact that steps on the substrate and steps of the film run in different directions and cannot be mistaken. The evolution of surface structure of the KBr/InSb system, with increasing dose of KBr, imaged using STM is shown in Fig. 2:

The surface covered with ~0.75 ML KBr is shown in Fig. 2a. Atomically flat KBr layer growing in a 2D mode is seen as the bright areas.

Since the substrate and the film are unequivocally epitaxially matched, there are no faults during coalescence of KBr islands, formed on the surface for submonolayer coverages. The preferred crystallographic direction of 2D KBr edges is [110] and the morphology of the growing film indicates that the diffusion of KBr molecules along [110] direction is preferred, in agreement with previous studies [13,14]. The first KBr layer acts as a wetting layer; diffusivities of KBr molecules on top of the layer are very large, making it highly unlikely that the next level KBr islands would be formed before the first layer is completed [14].

Further growth of KBr on the surface proceeds in an almost perfect layer-by-layer growth and is essentially a homoepitaxy process. The n + 1*th* KBr monolayer growth proceeds through the formation and percolation of rectangular islands having their edges parallel to [100] and [010] crystallographic directions (electrically neutral edges in the rocksalt structure) as seen in Fig. 2b.The incomplete layer-by-layer growth for the system has been reported before, for the same substrate temperature during deposition as in this study (T = 100 °C) and similar procedure used for the clean surface preparation, resulting in the comparable initial step density on the InSb surface. [15] It is associated with the Ehrlich-Schwoebel barriers trapping KBr molecules on top of the islands, resulting in the frequent observation of the nucleation of a n + 1-*th* monolayer on top of the rectangular islands, before the completion of the n *th* monolayerHowever, the use of lower growth rates resulted in the significant reduction of this effect. While we have observed some cases of the nucleation of the n + 1-th layer before the full formation of the n-th layer, as shown in Fig. 2c., in most cases we observed the layer-by-layer growth. Thus, we can safely assume that, for samples used in this study described by integer number coverages (n = 2ML, 3ML, 4ML), the nominal coverages correspond to the real ones on most of the sample surface and only minor regions are covered by the thicker (n + 1 ML) and the thinner (n-1 ML) films.

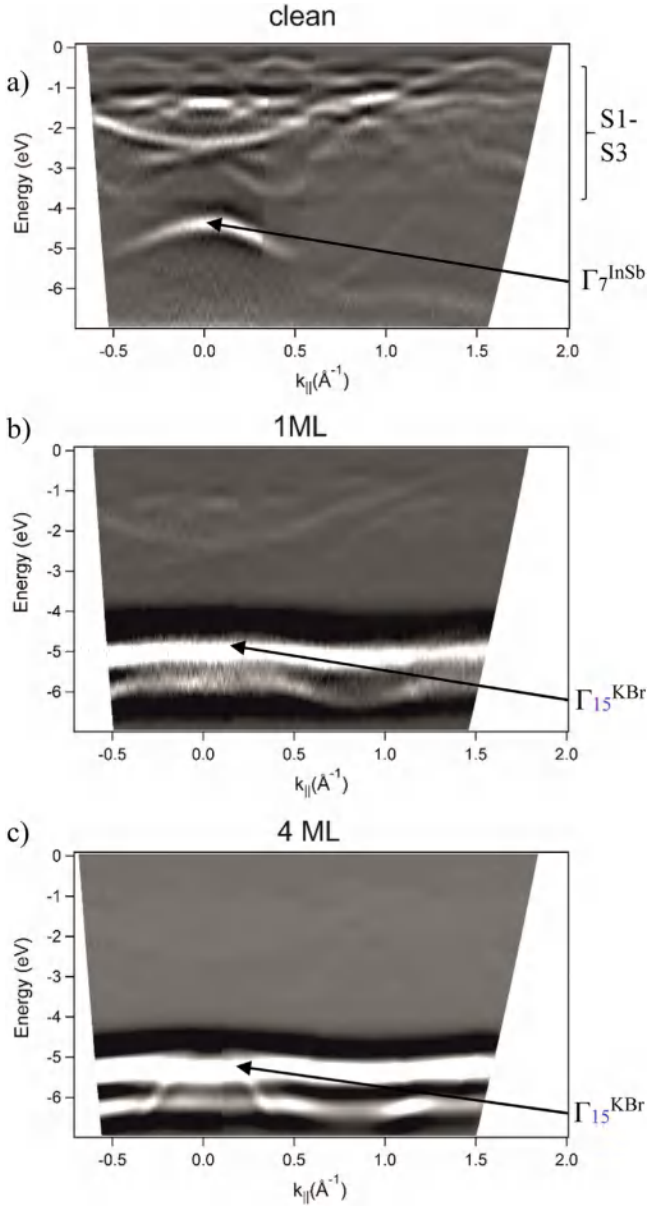

Fig. 3. ARPES spectra measured alongside ΓJ direction for the a) clean InSb sample, b) sample covered with 1ML of KBr, c) sample covered with 4ML of KBr. The spectra are presented as a second derivative of the original spectroscopic data. Signal intensity in different parts of the spectra can vary because of the matrix-elements effects.

The wetting layer (1 ML) is a special case and we have observed its complete formation before growth of consecutive layers, as described before. This is a very important observation since for coverages equal to 1 ML, no substrate surface should remain exposed. However, to ensure that, the data shown in the rest of the article, described as data from 1ML KBr coverage will actually come from the samples with the KBr dose slightly exceeding 1ML.

3.2. Surface electronic structure – ARPES

Fig. 3 shows the evolution of the ARPES spectrum of the InSb (001) surface covered with increasing coverage of KBr, measured alongside direction of the InSb (001) surface reciprocal lattice

The band structure of the clean sample is consistent with literature and its details have been described elsewhere [16]. It is

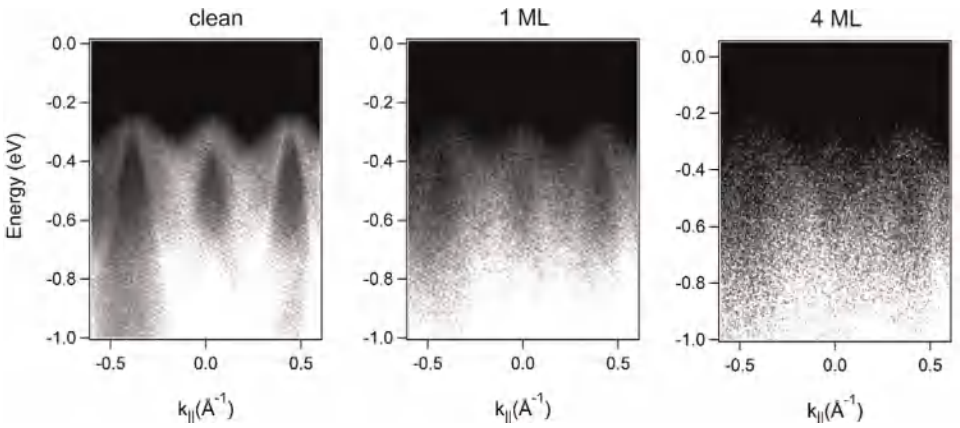

Fig. 4. ARPES spectra of the S1 surface state measured along Γ-J direction for a) clean InSb and surface with b) 1ML KBr coverage and c)4ML KBr coverage.

characterized by the existence of strong surface resonances: S1, S1′, S2, S2′, S3, S3′ in the energy range from 0 to −2 eV.

The Γ_7^{InSb} bulk band is observed at $E_B = 5{,}2$ eV for $k_{||} = 0$, in agreement with earlier studies[17]. Deposition of KBr on the surface results in the formation of a Γ_{15}^{KBr} valence electronic band [18], which is located at around the energy of E = −5 eV (although its exact position varies for coverages smaller than 2ML, which will be discussed later). Its formation is accompanied by the decreased intensity of the bands associated with InSb surface, due to the attenuation of the photoelectrons in the KBr layer. For coverages higher then 2ML, only electronic bands associated with KBr remain visible in the spectrum.

It is worth noting, that while the intensity of the electronic bands characteristic for the c(8 × 2) reconstruction (S1- S3 resonance bands) decreases with increasing KBr coverage, the band shapes remain unaffected by the overlayer. This is further evidenced in Fig. 4, which shows ARPES spectra taken, near the Fermi level of the (a) clean InSb sample (b) sample covered with 1ML KBr and (c) sample covered with 4ML KBr. Symmetry and periodicity of the S1 surface resonance, present in this region, remain unchanged.

Analysis of the energy spectra taken in the Γ point of the reciprocal lattice for varying KBr coverage is shown in Fig. 5

The results show that the position of Γ_{15}^{KBr} band shifts to the lower energy by 0.2 eV when the KBr coverage changes from 1 ML to 2 ML which is likely associated with a change in the localization energy of KBr electrons. For higher coverages no differences in the photoelectron spectra were observed. Thus the KBr films appears to achieve bulk-like electronic properties already at coverages of 2ML.

3.3. *InSb- KBr interface electronic structure and the dielectric hypothesis*

For the interpretation of STM images it is important to investigate band alignment of KBr/InSb(001) interface. Simple scheme of such alignment is shown in Fig. 7.

The positions of the valence band maxima of InSb and KBr can be obtained directly from ARPES measurements (see Fig. 3). The values of the bandgap energy of InSb (∼0.23 eV at 80 K [19]) and of KBr (∼7.6 eV [20]) are known, allowing for the precise analysis of band alignment. This is possible, because, as was discussed in section 3.2, the thin KBr overlayer achieves bulk-like properties already at the coverage of 2ML, making it possible to the bulk parameters. As seen in Fig. 3, for the KBr layer, the measured dispersion $E(k_{||})$ is rather weak (< 0.5 eV) which is clearly understandable in light of the fact that the KBr electrons are best described as localized on atoms (due to almost pure ionic bonds). Because the dispersion $E(k_{|})$ [along (001)] must be the same as $E(k_{||})$ measured [along (100)], the

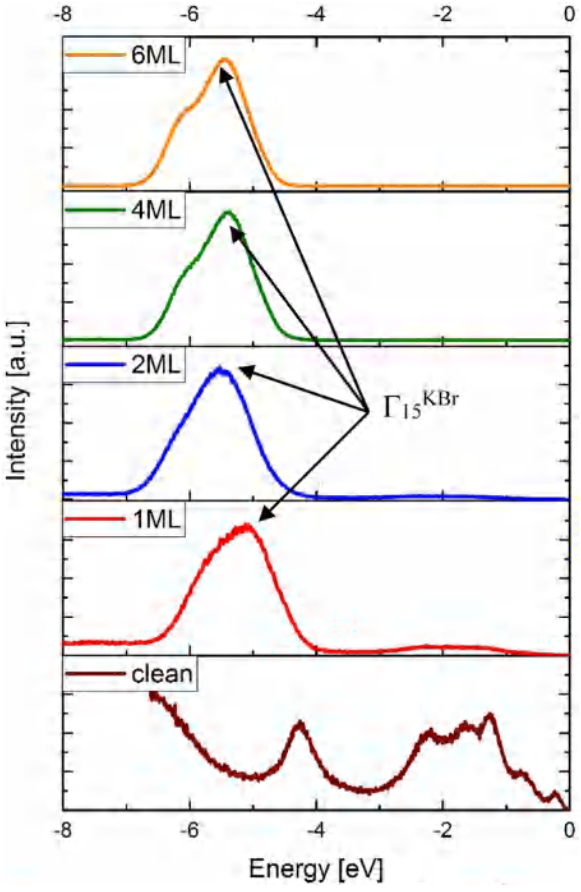

Fig. 5. Energy spectra measured along the normal to the surface (in the gamma point of the reciprocal lattice) for varying KBr surface coverage (indicated for each spectrum).

bands shown in Fig. 6 visualize the KBr valence band on the energy scale to within 0.5 eV accuracy.

Because the Fermi levels of the three components are aligned, the conduction band minimum (CBM) of KBr, far from the InSb-KBr interface, is located at the energy around 2.6 eV higher then CBM of InSb while the valence band minimum of KBr is located at energy around 5 eV lower than the VBM of InSb. As was shown before, for coverages higher or equal to 2ML, the band structure of KBr reaches the bulk-like limit and the band-bending effects are not present at the surface.

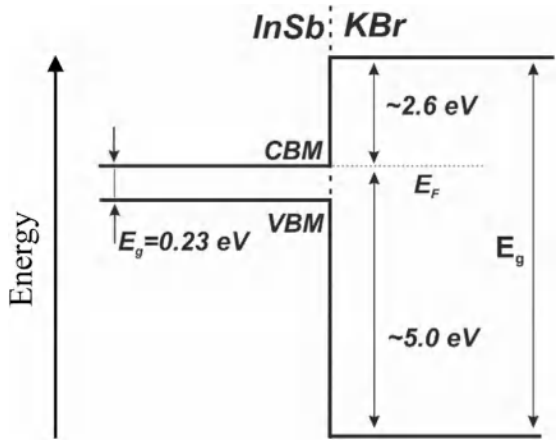

Fig. 6. Band alignment diagram for KBr/InSb(001) system at T = 80 K.

The interpretation of STM patterns often relies on using computational methods, in particular DFT, to simulate images for given surface structures and bias voltages and comparing them with observed data. This method is, however, not applicable to all cases, as it relies on the prior knowledge of the surface structure, ignores the real tip electronic structure using Tersoff-Hamman (density of states) approximation and can be difficult to apply for very low electron densities, as in the present case. Although it is tempting to model the system as closely as possible, we have decided to use the simplest feasible approach due to complexity of our sample, in the context of tunneling processes.

Our approach is based on the experimentally determined electronic structure of the surface. As we have shown earlier (see Section 3.2), the electronic structure of the c(8 × 2) reconstruction remains largely unaffected by the growth of KBr layer. Therefore, in the first approximation, the STM tip – KBr – InSb surface system can be treated as a semiconductor (InSb) – double dielectric layer (KBr, vacuum) – metal (tip) system. This assumption will be referred to as the "dielectric hypothesis". From the band alignment analysis (see Fig. 6), we can see that it should be valid for the sample bias voltages in the range from −5 eV to +2.6 eV (this is a rough estimation – see Fig. 7 for more detailed analysis of the situation with the presence of bias voltages), where the only non-zero density of electronic states is present at the KBr – InSb interface (with the exception of a narrow bandgap of InSb); this scenario will be referred to as the "bandgap imaging regime". If we utilize bias voltages well outside this range, the tunneling current will flow through electronic states of the KBr film.

We may treat this situation with a simple mathematical model, in which the tunneling current has to be transmitted through the potential barrier composed of the two parts (associated to KBr layer and vacuum between the tip and the surface of the sample). The scheme of such situation is drawn in Fig. 7.

One of the most easily observed parameters in the STM images is the apparent step height. In order to test the dielectric hypothesis, we will now calculate the apparent step-height of KBr layer for the STM measurements performed inside the "bandgap imaging regime", using the dielectric hypothesis and compare the predictions with the experimental data. For simplicity we assume that the tunneling barrier is rectangular (which will work best for low and moderate bias voltages)

In our STM measurements we have used the topographic imaging mode (constant-current mode). The tunneling current dynamics through a simple, rectangular barrier is dominated by transmission probability T:

$$T \sim \exp(-\alpha d) \tag{1}$$

where d is the barrier width and α is the attenuation coefficient defined as:

$$\alpha = \frac{2\sqrt{2mV}}{\hbar} \tag{2}$$

where m is the effective electron mass in the dielectric and V is the barrier height. The transmission probability through the barrier, composed of two different dielectrics, is the product of transmission probabilities for each of these layers: $T = T_1T_2$.

To obtain apparent step height in STM images, we have to compare the transmission probabilities on the two sides of crystalline dielectric step of the *true* height a, described by the set of parameters: $(V_1, V_2, m_1, m_2, T_{low} = T_1, T_2, d_1 = na, d_2)$ on the "low side", and $(V_1, V_2, m_1, m_2, T_{high} = T_1', T_2', d_1' = (n+1)a, d_2')$ on the "high side".

In the constant current mode, we require that:

$$T_{low} = T_{high} \tag{3}$$

$$T_1T_2 = T_1'T_2' \tag{4}$$

and obtain immediately:

$$d'_2 = d_2 - \frac{\sqrt{m_1V_1}}{\sqrt{m_2V_2}}a \tag{5}$$

the apparent *STM step height* Δ is then obtained as:

$$\Delta = d'_1 + d'_2 - d_1 - d_2 - = \left(1 - \frac{\sqrt{m_1V_1}}{\sqrt{m_2V_2}}\right)a \tag{6}$$

For V_1 = 2.8 eV (a difference between valence band maximum of InSb and conduction band minimum of KBr, see Fig. 6), V_2 = 4.6 eV (work function of InSb [21]) and electron effective mass in KBr equal to $m^* = 0.46m_e$ [20] we obtain apparent step height equal to 1.7 Å.

Thus, within the dielectric hypothesis the step on crystalline dielectric layer is in most cases imaged by STM as a step, however its height, in general, will differ from the true step height.

We have performed studies of STM step heights on InSb and KBr film surfaces. The results are shown in Table 1:

Apparent step heights between subsequent KBr layers measured inside the "bandgap imaging regime" (see Table. 1), are around 1.7 Å, which agrees well with the predictions of our simple model. If the value U_{bias} is higher than around 3 V and the imaging takes place outside the "bandgap imaging regine" the observed STM step heights are within the range of 3.0-3.6 Å step regardless the applied bias voltage. KBr has its lattice constant ~6.58 Å, consequently the single monolayer of KBr will have, on the (001) face, the height of around 3.29 Å. This is consistent with results obtained for U_{bias} = 3.5 V and U_{bias} = 4.0 V (outside the "bandgap imaging regime").

Our results show that STM is imaging the surface of KBr film, if U_{bias} is set to high positive values, i.e. when KBr conduction states at the surface of the film become available for tunneling electrons (see Fig. 7b for the relevant band diagram). The minimal U_{bias} over which this imaging regime is possible is likely around 3.0 eV – we are not able to give very precise value both due to the uncertainties both in the band alignment and in the parameter ΔV_1 - see Fig. 7.

3.4. Interpretation of high-resolution STM images using dielectric hypothesis

Fig. 8 shows the high-resolution STM images of the InSb surfaces with varying KBr coverage, imaged for the bias voltages ranging from −2 V to −4 V ("bandgap imaging regime"):

The atomically resolved images obtained within the "bandgap imaging regime" are very different for various KBr coverages. This is not explained directly with the "dielectric hypothesis" description. For the coverages of 1ML and 2ML, c(8 × 2) symmetry is visible

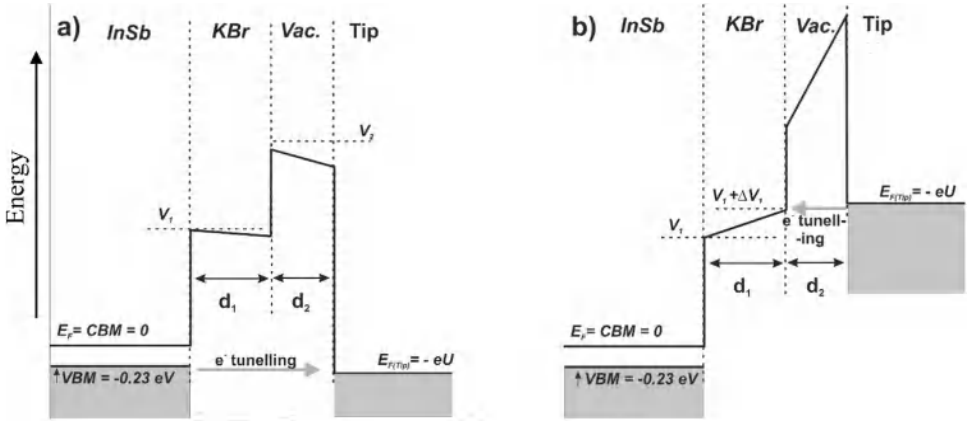

Fig. 7. Diagrams explaining the situation occurring for tunneling in two regimes a) tunneling through the KBr bandgap for negative sample bias and b) tunneling to the conduction band of KBr for positive sample bias. Shadowed areas denote occupied electronic states.

Table 1
STM apparent step hights in Å, obtained for different bias voltages, averaged over 2–5 different samples/tips. In all cases single results are within ±0.2 Å from the shown averages. InSb substrate step heights are included to show the correct scanner calibration. The bilayer step height on (001)InSb surface is equal to 6.48 Å.

Bias voltage [V]	−1.0 V	−2.0 V	−2.5 V	−3.0 V	+2.0V	+2.5	+3.5	+4.0
InSb n/n + 1		3.3			3.3			
KBr 1/2	1.7	1.9	1.7	1.7	2.0	2.1	3.5	3.6
KBr 2/3		1.8	1.7	1.7	1.6	1.5	3.1	3.3
KBr 3/4		1.8	1.8	1.7	1.6	1.6	3.0	3.3

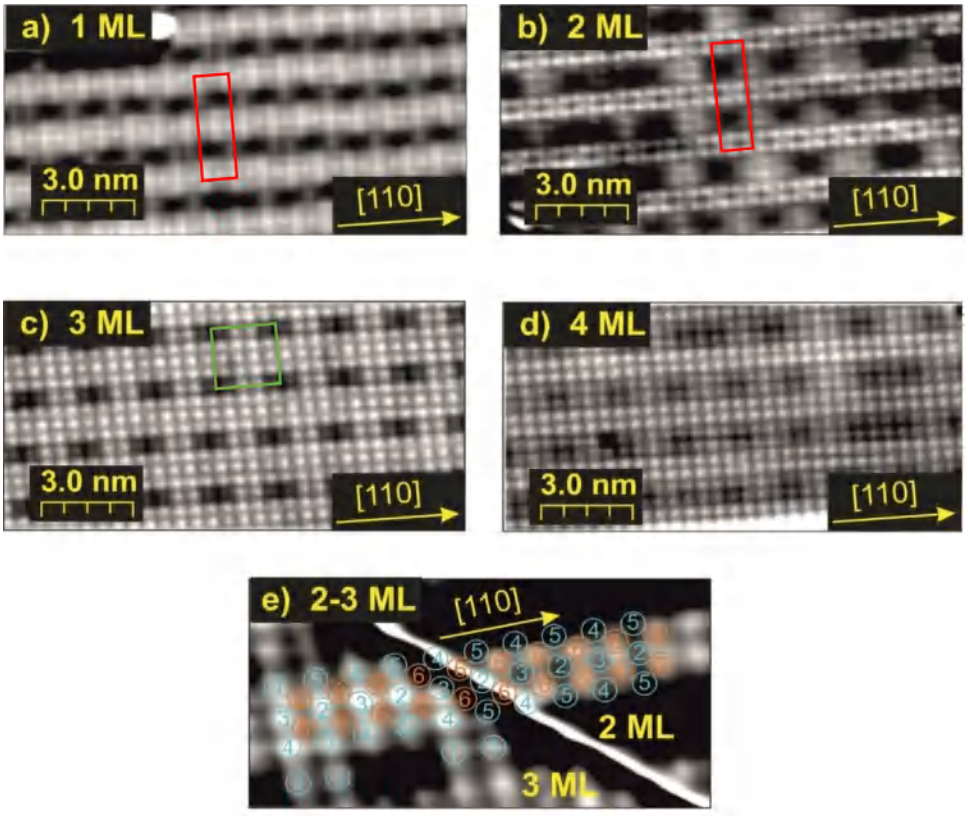

Fig. 8. STM images of InSb surfaces with varying KBr coverage: a) 1ML KBr/InSb(001), imaged with the constant current mode at 25 pA tunneling current, and sample bias −4.0 V (similar patterns were seen within the range from −2.0 to −4.0 V sample bias), b) 2ML KBr/InSb(001) imaged with the constant height mode, at 50 pA tunneling current, and sample bias −2.0 V (similar patterns were seen within the range from −1.5 to −4.0 V sample bias), c) 3ML KBr/InSb(001)imaged with the constant height mode at 50 pA tunneling current, and sample bias −2.5 V (similar patterns were seen also at −2.0 V and −3.0 V sample bias), d) 4ML KBr/InSb(001) imaged with the constant height mode at 10 pA tunneling current, and sample bias −3.0 V, e) Transition between the 1ML and 2 ML patterns. The grayscale has been manipulated nonlinearly (flattened) to show clearly two relatively shallow patterns imaged at different heights and the white line is an artifact resulting from this manipulation. The numbers denote surface lattice (top layer) atoms following the convention proposed by Kumpf et al., 1,2,3,4,5 s correspond to In atoms and 6 s correspond to Sb atoms.

(marked by red rectangles), while for coverages of 3ML and 4ML a grainy (1×1) structure appears, albeit it is also modulated strongly. A partially disordered (4×4) pattern comprised of dominant dark voids is visible – marked by green rectangle for coverage of 3ML in Fig. 8c.

The association of the characteristic patterns with the film thicknesses is based on the analysis of several STM images, showing transitions between consecutive KBr film thicknessess of **n** and **n + 1** monolayers (observed for fractional coverages – see for example Fig. 8b, where we observe islands covering about 50% of surface, having the pattern seen in Fig. 8b. appearing on the background having the pattern 7.a). At steps we observe the alignment of two different patterns – see example shown in Fig. 8e (alignment of the patterns observed for 2ML and 3ML coverage). Analysis similar to the one illustrated in Fig. 8e has been done also for steps Substrate/1 ML, 1 ML/2ML, 3ML/4ML. Thus, the alignment is found between the pattern characteristic for the KBr film of any given thickness up to 4 ML and the well-known substrate structure [18].

Let's start our discussion with the 2 ML coverage case. The dominant bright features (constituting double rows in STM images) are located directly over the positions of Sb6 atoms (cf. Fig. 8b, e), expected for the clean, In-rich, $c(8 \times 2)$ surface reconstruction of InSb [22]. For the 3 ML coverage (cf. Fig. 8c, e) the bright spots constituting triple rows, are located over the positions of In2, In3, In4, and In5 atoms expected for the same clean surface. We have marked the positions of these atoms expected from the model of the clean, $c(8 \times 2)$ – reconstructed surface on Fig. 8e and the analysis shows remarkable agreement of the features observed on KBr-covered surfaces with the model of a clean surface.

Considering the row occupancy and included symmetries, remaining bright spots seem to be located over rearranged In1 atoms, which are the special case here. On the clean InSb these rows do not have atomic sites in a form of deep energy minima – the rows are observed fluctuating at temperatures as low as 120 K [23]. Therefore the In1 atoms under KBr film will most likely stay confined to the row, but might be found at different positions as compared with the ground-state free surface. The occupation of In1 row is less than 100% and the non-occupied In1 sites appear to form the observed (4×4) symmetry, with some phase differences between different In1 rows.

For the 1 ML coverage the pattern is not well resolved, however, the visible wide modulated stripes are located over In2, In3, In4, and In5 substrate atoms and included symmetries agree. For the 4 ML coverage the dominant bright features (in double rows) are seen again over Sb6 atoms. The remaining darker features are seen over bridge positions between Sb7 and Sb8 atomic sites.

These results show clearly that our atomically resolved STM patterns of KBr – covered InSb(001) reflect mostly the interface structure, but the KBr film, depending on its thickness enhances either the In sublattice features (for odd number of layers), or Sb sublattice features (for even number of layers).

This turns our attention back to the "dielectric hypothesis" since it in obvious way explains why the interface structure is observed. However, some corrections are needed to account for the variability of the observed patterns at changing coverages. It is likely that they may be introduced as small corrections rather than substantial changes in the "dielectric hypothesis", because the atomically resolved modulation, in recorded constant current STM images, is small compared to the apparent step height. This is shown in Fig. 9.

While we cannot definitely explain what the postulated corrections are, we have identified two possibilities that may be discussed in terms of simple models. The first one assumes that the binding between the substrates is purely ionic therefore their electronic systems are decoupled. In such case the KBr film acts as ideal dielectric layer but, at the considered scales, one cannot neglect its atomic structure.

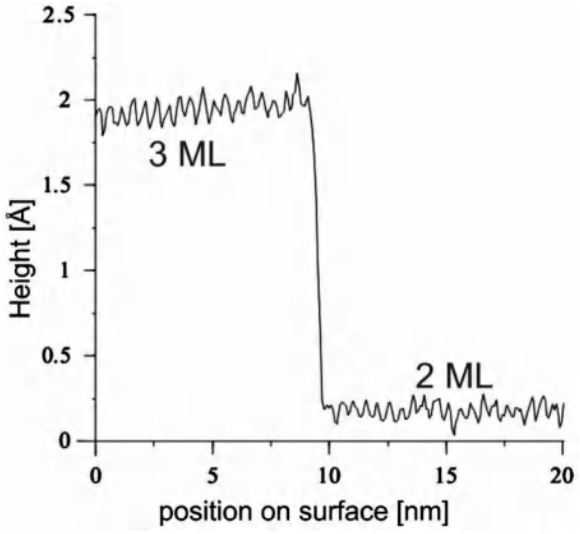

Fig. 9. An example of a constant tunneling current height profile (acquired in topographic STM mode) in the proximity of 2/3ML step on KBr/InSb ultrathin film. Atomically resolved modulation amplitude corresponds to less than 10% of the apparent step height.

The tunneling barrier, constituted by the film, is spatially modulated in the sample plane in register with KBr crystal structure, (alternating positions of K^+ and Br^- ions), which is coupled to the substrate/interface structure. We observe tunneling current maxima only when the STM tip is over Br atoms/ions of the film (which are located directly over In atoms for the odd number of KBr layers and directly over Sb atoms for the even number of KBr layers). Thus it is likely that, through simple electrostatics, ultrathin KBr film acts as an atomic "sieve" facilitating, depending on the film thickness, tunneling to the given interface sublattice.

The other possibility involves quantum-mechanical phenomena, such as hybridizing electron wavefunctions of KBr and InSb, in a way that couples the electronic states of the substrate with the KBr film. This would create electronic states in the thin KBr layer, which could facilitate the tunneling current. The density of these states should be very low so that the current flowing through these states could be described as a minor correction to the total tunneling current.

Despite the need of introducing certain corrections to account for the atomic-scale effects, which is beyond the scope of this paper, it appears that our simple approach for the interpretation of STM patterns of the studied system is, in principle, correct. Using "bandgap imaging mode" (bias voltage chosen so that the Fermi level of the tip lays is located within the bandgap of KBr), we were able to image the structure of the interface between KBr and InSb. This interpretation does not explain why either In or Sb sub-lattice was imaged depending on KBr coverage, but yields valuable information about the structure of the system.

The interphase structure studied by STM is very similar to the structure of the clean, In-rich, $c(8 \times 2)$ surface reconstruction of InSb, but with additional, disordered, (4×4) periodicity due to reordering of the substrate In1 rows. This conclusion is further supported by the fact that both LEED and APRES studies have revealed, that the $c(8 \times 2)$ periodicity remains rather unperturbed by the deposition of KBr layer (see Figs. 1 b, 3 b, 4 b).

4. Conclusions

We have studied thin KBr films on the $c(8 \times 2)$, In-rich (001) InSb surface. We have found that the formation of the KBr film does not perturb atomic and electronic structure of the substrate. KBr film

achieves bulk-like electronic properties already at the coverage of 2ML, becoming effectively a quasi-2D dielectric.

We have constructed a simple model of the electronic structure of the KBr/InSb surface and used this model to interpret the STM images obtained for the system. We show that, for sample bias voltages in the range roughly from −5 eV to +3 eV (when the Fermi level of the tip is located within the bandgap of KBr) the KBr film can be treated simply as a dielectric layer, modifying the potential barrier for the tunneling electrons. Thus, we have imaged directly the atomically-resolved structure of the KBr-InSb interface. The interface shows typical characteristics of the c(8×2) reconstructed, clean InSb(001) surface. We have also observed an interesting effect, where the In sublattice of the interface is visible in the STM images only for the odd number of KBr layers, while the Sb sublattice of the interface is visible only for the even number of KBr layers. This is explained by assuming atomic scale modulation of the tunneling barrier height by the crystallographically ordered ionic film. However, we do not exclude that quantum-mechanical wavefuction mixing (of the substrate and the film) can also play some role here.

Presented approach may be applicable to other similar systems, where insulating layer is thin enough to allow tunneling of electrons to/from the substrate. It may be used as a good starting point towards more complex, detailed models.

Acknowledgements

We acknowledge financial support by Polish National Science Centre (NCN) (contract 2011/03/B/ST3/02070) and by Polish National Leading Research Centre “Matter-Energy-Future”. The research was carried out with the equipment purchased thanks to European Regional Development Fund in the framework of the Polish Innovation Economy Operational Program (contract no. POIG.02.01.00-12-023/08). We want to thank Grzegorz Goryl for his invaluable help with STM imaging and interpretation.

References

[1] R. Chau, S. Datta, A. Majumdar, Opportunities and challenges of III?V nanoelectronics for future high-speed, low-power logic applications, IEEE Compound Semiconductor Integrated Circuit Symposium, 2005. CSIC ‘05 (2005) 4, http://dx.doi.org/10.1109/csics.2005.1531740.
[2] M. Edirisooriya, T.D. Mishima, C.K. Gaspe, K. Bottoms, R.J. Hauenstein, M.B. Santos, InSb quantum-well structures for electronic device applications, J. Crystal Growth 311 (2009) 1972–1975.
[3] Yu. A. Goldberg, in: M. Levinshtein, S. Rumyantsev, M. Shur (Eds.), Handbook Series on Semiconductor Parameters, vol.1, World Scientific, London, 1996, pp. 191–213.
[4] Intel News Fact Sheet, IEEE International Solid-State Circuits Conference (ISSCC), 2015, http://download.intel.com/newsroom/kits/isscc/2015/pdfs/Intel_ISSCC_factsheet.pdf, (Accessed 30 January 2017).
[5] S. Anthony, Intel forges ahead to 10 nm, will move away from silicon at 7 nm, Ars Technica, 23.02.201, 2015, arstechnica.com/gadgets/2015/02/intel-forges-ahead-to-10nm-will-move-away-from-silicon-at-7nm/ (Accessed: 30 January 2017).
[6] Jesús A. del Alamo, Nanometre-scale electronics with III–V compound semiconductors, Nature 479 (2017) 317–332, http://dx.doi.org/10.1038/nature10677.
[7] J.B. Robertson Falabretti, Band offsets of high K gate oxides on III-V semiconductors, J. Appl. Phys. 100 (014111) (2006).
[8] T.V. Lvova, A.L. Shakhmin, I.V. Sedova, M.V. Lebedev, Sulfur passivation of InSb (100) surfaces: Comparison of aqueous and alcoholic ammonium sulfide solutions using X-ray photoemission spectroscopy, Appl. Surf. Sci. 311 (2014) 300–307, http://dx.doi.org/10.1016/j.apsusc.2014.05.058.
[9] J.J. Kolodziej, B. Such, P. Czuba, F. Krok, P. Piatkowski, M. Szymonski, Scanning-tunneling/atomic-force microscopy study of the growth of KBr films on InSb(001), Surf. Sci. 506 (1–2) (2002) 12–22.
[10] Tomonori Nishimura, Koji Kita, Akira Toriumi, Evidence for strong Fermi-level pinning due to metal-induced gap states at metal/germanium interface, Appl. Phys. Lett. 91 (1-3) (2007) 123.
[11] G.M. Rutter, N.P. Guisinger, J.N. Crain, E.A.A. Jarvis, M.D. Stiles, T. Li, P.N. First, J.A. Stroscio, Imaging the interface of epitaxial graphene with silicon carbide via scanning tunneling microscopy, Phys. Rev. B 76 (2007) 235416, http://dx.doi.org/10.1103/PhysRevB.76.235416.
[12] P. Han, A.R. Kurland, A.N. Giordano, S.U. Nanayakkara, M.M. Blake, C.M. Pochas, P.S. Weiss, Heads and tails: simultaneous exposed and buried interface imaging of monolayers, ACS Nano 3 (2009) 3115–3121, http://dx.doi.org/10.1021/nn901030x.
[13] F. Krok, J.J. Kolodziej, B. Such, P. Czuba, P. Struski, P. Piatkowski, M. Szymonski, Dynamic force microscopy and Kelvin probe force microscopy of KBr film on InSb(001) surface at submonolayer coverage, Surf. Sci. 566 (2004) 63–67, http://dx.doi.org/10.1016/j.susc.2004.05.023.
[14] S. Godlewski, G. Goryl, J.J. Kolodziej, M. Szymonski, KBr superstructure templates self-assembled on reconstructed AIIIBV semiconductor surfaces, Appl. Surf. Sci. 256 (2010) 3746–3752, http://dx.doi.org/10.1016/j.apsusc.2010.01.018.
[15] J.J. Kolodziej, B. Such, P. Czuba, F. Krok, P. Piatkowski, M. Szymonski, Scanning-tunneling/atomic-force microscopy study of the growth of KBr films on InSb(001), Surf. Sci. 506 (2002) 12–22, http://dx.doi.org/10.1016/S0039-6028(02)01438-3.
[16] L. Walczak, G. Goryl, M.A. Valbuena, I. Vobornik, A. Tejeda, A. Taleb-Ibrahimi, J.J. Kolodziej, P. Segovia, E.G. Michel, Surface electronic structure of InSb(001)-c(8×2), Surf. Sci. 608 (2013) 22–30, http://dx.doi.org/10.1016/j.susc.2012.09.009.
[17] J.R. Chelikowsky, M.L. Cohen, Nonlocal pseudopotential calculations for the electronic structure of eleven diamond and zinc-blende semiconductors, Phys. Rev. B 14 (1976) 556–582, http://dx.doi.org/10.1103/PhysRevB.14.556.
[18] D.B. Sirdeshmukh, L. Sirdeshmukh, K.G. Subhadra, Alkali Halides: A Handbook of Physical Properties, Springer Series in Materials Science, Springer-Verlag Berlin Heidelberg GmbH, 2001, ISBN 978-3-642-07578-0.
[19] C.L. Littler, D.G. Seiler, Temperature dependence of the energy gap of InSb using nonlinear optical techniques, Appl. Phys. Lett. 46 (1985) 986–988, http://dx.doi.org/10.1063/1.95789.
[20] Page, E. Hygh, Calculation of energy bands in alkali halides, Phys. Rev. B 1 (1970) 3472–3479.
[21] D. Haneman, Photoelectric emission and work functions of InSb, GaAs, Bi2Te3 and germanium, J. Phys. Chem. Solids 11 (1959) 205–214, http://dx.doi.org/10.1016/0022-3697(59)90215-X.
[22] G. Goryl, O. Boelling, S. Godlewski, J.J. Kolodziej, B. Such, M. Szymonski, Low temperature InSb(001) surface structure studied by scanning tunneling microscopy, Surf. Sci. 601 (2007) 3605–3610, http://dx.doi.org/10.1016/j.susc.2007.07.002.
[23] G. Goryl, D. Toton, N. Tomaszewska, J.S. Prauzner-Bechcicki, L. Walczak, A. Tejeda, A. Taleb-Ibrahimi, L. Kantorovich, E.G. Michel, J.J. Kolodziej, Structure of the indium-rich InSb(001) surface, Phys. Rev. B 82 (165311) (2010), http://dx.doi.org/10.1103/physrevb.82.165311.